PERGAMON

Energy Conversion and Management 42 (2001) 995–1022

ENERGY CONVERSION & MANAGEMENT

www.elsevier.com/locate/enconman

Application of solar assisted heating and desiccant cooling systems for a domestic building

Khalid A. Joudi *, Nabeel S. Dhaidan

Department of Mechanical Engineering, College of Engineering, University of Baghdad, Baghdad, Iraq

Received 22 February 2000; accepted 9 September 2000

Abstract

The performance of solar assisted heating and desiccant cooling systems for a domestic two story residence located in Baghdad was evaluated. A computer simulation was developed to assess the effects of various designs and operating conditions on the performance of the system and its components. The solar air heating system included a V corrugated solar air heater array, a rock bed storage unit and an auxiliary heat source. A rotary silica gel desiccant dehumidifier, a sensible cooler and an evaporative cooler were added to the above system to form an open cycle solar assisted desiccant cooling system. The variable base degree-day method was employed in order to incorporate the hourly variations of solar heat gain and internal heat gains of the space in the estimation of the heating load. The transfer function method was used to evaluate the hourly variation of the cooling load.

Only two collector rows in series were employed to provide the required supply air temperature for the heating system and the required regeneration temperature for the desiccant cooling system. This array gave an air outlet temperature of approximately 62°C at an air mass flux of 0.06 kg/s m^2 at midday in July, while a 36°C outlet air temperature was achieved for the same array and mass flux in January.

The results of simulation of the solar air heating system indicated that the major design parameter is the collector area. The effect of air mass flux through the collector array was not significant. Also, increasing the rock bed storage volume produces only slight improvements in the solar fraction.

Simulation of the open cycle solar assisted desiccant cooling system showed that the ambient temperature, regeneration temperature, heat exchanger effectiveness and evaporative cooler effectiveness have major influences on the system performance, whereas the dehumidifier has a minor effect. Also, the simulated system was capable of providing a cool supply of air at acceptable comfort conditions for various summer days in Baghdad.

Keywords: Solar heating and cooling systems; Simulation of solar air heating system; Simulation of solar assisted desiccant cooling system; Modeling of solar array and shading effect

* Corresponding author.

0196-8904/01/$ - see front matter
PII: S0196-8904(00)00111-4

Nomenclature

A	collector width (m)
A_r	heat transfer area (m^2)
A_c	area of collector (m^2)
A_{rw}	area of glass window (m^2)
b_n	coefficients of transfer function
C	diffuse radiation factor
C_n	coefficients of transfer function (W/m^2 °C)
C_p	specific heat of air (J/kg K)
CFM	correction factor of intercept and slope to M collectors connected in series
COP	coefficient of performance
D	collector spacing (m)
d	Relative collector spacing
d_n	coefficients of transfer function
F_e	linear floor slab loss coefficient (taken as 1.4 [17]) (W/m °C)
F_i	combined heat and mass potential, $i = 1, 2$ (arbitrary dimensions)
F_R	collector heat removal factor
$F_{R1}(\tau\alpha)_1$	intercept of efficiency curve for single collector
$F_R(\tau\alpha)_M$	intercept of efficiency curve for M collectors in series
$F_{R1}U_{L1}$	slope of efficiency curve for single collector (W/m^2 °C)
$[F_R U_L]_M$	Slope of efficiency curve for M collectors in series (W/m^2 °C)
f	fraction of heating load supplied by solar energy
G	mass flux of air through collector (kg/s m^2)
H_c	collector height (m)
H_s	shadow height (m)
h_a	enthalpy of ambient air (kJ/kg K)
h_{sup}	enthalpy of supply air (kJ/kg K)
h_s	relative shadow height
h_0	coefficient of heat transfer by long wave radiation and convection (W/m^2 K)
I_{DN}	direct normal irradiance (W/m^2)
I_T	total solar irradiance (W/m^2)
I_{bs}	beam radiation on a shaded collector (W/m^2)
I_{TS}	total radiation on a shaded collector (W/m^2)
I_{ds}	diffuse radiation on a shaded collector (W/m^2)
$\overline{I}_T$	total monthly average – daily total radiation on a tilted surface (MJ/m^2)
L	collector row length (m)
L_T	monthly total heating load (J)
L_S	shadow length (m)
ℓ	relative collector row length
ℓ_s	relative shadow length
M	number of collectors in series
M_P	number of collectors in parallel
$\dot{m}_p$	flow rate of process air (kg/s)
$\dot{m}_{reg}$	flow rate of regeneration air (kg/s)
$\dot{m}_f$	mass flux of air through collector (l/s m^2)
$\dot{m}_c$	flow rate of air through collector (kg/s)
N	number of days in month
N_{ch}	number of air changes per hour
P_f	perimeter of floor (m)
Q_f	free energy of building (W)
Q_{floor}	heat loss from slab floor (W)
Q_{inf}	infiltration heat loss (W)
Q_L	heating load (W)
Q_{lig}	heat gain from lighting (W)
Q_{occ}	heat gain from occupants (W)
Q_{op}	solar heat gain through opaque surfaces (W)
Q_{sol}	solar heat gain through window (W)
Q_τ	cooling load (W)
q_τ	heat gain (W)
q_{av}	average heat flow (W/m^2)
r_s	relative shaded area
ΔR	difference between long wave radiation incident on surface from sky and surroundings, and radiation emitted

	by black body at outdoor air temperature (W/m^2)
S_c	shading coefficient
SHG	solar heat gain (W/m^2)
SHGF	solar heat gain factor (W/m^2)
T	temperature (K)
T_{sol}	sol–air temperature (°C)
$\overline{T}_{sol}$	average sol–air temperature (°C)
T_b	base temperature (°C)
$\overline{T}_b$	average base temperature (°C)
T_{sp}	indoor space temperature (°C)
T_a	ambient temperature (°C)
$\overline{T}_a$	average ambient temperature (°C)
T_{ref}	reference temperature (100) (°C)
$T_{p,o}$	temperature of process air leaving heat exchanger (°C)
$T_{p,i}$	temperature of process air entering heat exchanger (°C)
$T_{e,o}$	temperature of process air leaving evaporative cooler (°C)
$T_{w,i}$	temperature of cooled water entering evaporative cooler (°C)
$T_{ew,i}$	wet bulb temperature of process air entering evaporative cooler (°C)
T_{reg}	regeneration temperature (°C)
T_{out}	outlet air temperature from collector array (°C)
T_{sup}	supply air temperature (°C)
Δt	total seconds in month (s)
U	heat transfer coefficient (W/m^2 °C)
U_L	collector heat loss factor (W/m^2 °C)
UA	overall energy loss coefficient–area product of building (W/°C)
$(UA)_s$	overall energy loss coefficient–area product of opaque surfaces (W/°C)
V	volume of building (m^3)
V_s	storage capacity per collector area (m)
X	dimensionless parameter
X_c	corrective dimensionless parameter
Y	dimensionless parameter
W	Moisture content (kg/kg dry air)
$w_1, w_2, \ldots$	coefficients of room transfer function
Greek symbols	
α	solar altitude angle (degree)
α_0	absorptivity of wall or roof
β	collector tilt angle with horizon (degree)
γ_s	solar azimuth angle (degree)
ε_s	Hemispherical emittance of surface
η_{F_i}	F_i efficiency of dehumidifier $i = 1, 2$
η_{hx}	heat exchanger effectiveness
η_{ev}	evaporative cooler effectiveness
θ	solar radiation incident angle (degree)
ρ	density of air (kg/m^3)
ρ_g	ground reflectivity
$(\overline{\tau\alpha})$	monthly average transmittance–absorptance product
v_0, v_1	coefficients of room transfer function

1. Introduction

One of the major applications of solar energy today is for providing space heating and air conditioning of buildings. A solar system is composed of three basic elements, the solar collector array, the thermal storage subsystem and the load. It is technically possible to build a solar system which could supply the total heating load of the building and achieve the required regeneration energy for a solar assisted desiccant cooling system, but this system is accompanied with an economic penalty. Thus, most solar systems consist of a combination of solar and auxiliary sources.

There are two ways for predicting the performance of solar heating systems. One is the detailed simulation techniques, such as TRNSYS [1], which is suitable for large and non-standard systems, and the other is simplified method known as the *f*-chart method [2], which is used for standard systems where the cost of detailed simulations cannot be justified. The *f*-chart method is simple in use and requires only monthly average meteorological data. Kreider and Kreith [3] indicated that the performance predictions of the *f*-chart method have been compared with predictions made by very detailed simulations in 14 locations in the United States, and the standard error of the difference between the simulation and the *f*-chart results was about 2.5%. Ajona and Gordon [4] introduced the analytical model for predicting solar heating system performance. The effect of stratification in packed rock bed storage was explicitly taken in to account. Although this model is not as simple as the *f*-chart method, it offers the dependence of system performance on all important system and climatic variables by their monthly average value and by replacing a monthly calculation by a calculation for one repetitive average day. They reported very good agreement between the *f*-chart method and their analytical model. Duffie and Mitchell [5] deduced that there was a general trend of agreement between the measured and predicted fraction of load met by solar energy. The measured solar contribution is based on measured meteorological conditions. The bias between the predicted and measured performance can be interpreted due to the small number of measured data points. Systems with configurations close to the standard system show good agreement between predicted and measured performance, while those with significant differences do not.

Solar cooling of buildings is a significant application of solar energy. Cooling load and availability of solar radiation are approximately in phase. The combination of solar cooling and heating should improve the economics compared to heating or cooling alone. Dunkle [6] proposed a desiccant cooling cycle where the desiccant regeneration is performed by a solar air heater. A pebble bed storage unit may be used for providing regeneration energy during periods of inadequate or no solar radiation. This cycle can be operated in humid, tropical or subtropical areas. Nelson et al. [7] discussed two modes of system operation. One is the ventilation mode, and the other is the recirculation mode. Seasonal simulation of the two modes showed the auxiliary energy requirements for the ventilation mode was about half that for the recirculation mode, hence its coefficient of performance was larger. Leersum [8] derived closed form expressions for the coefficient of performance for the Dunkle, ventilation, and recirculation cycles under a fairly broad set of assumptions. These expressions predict system performance trends observed in more complex models and allow the sensitivity of system performance to cycle air states, dehumidifier effectiveness and evaporative cooler effectiveness to be assessed. Kang and Maclain-Cross [9] discussed the advanced cycle which uses a finned coil heat exchanger-cooling tower combination for the ventilation and recirculation modes. The results showed that at ARI conditions, the coefficient of performance of these cycles was more than double that of the basic ventilation cycle. Also, they studied the effects of ambient and room temperatures on the coefficient of performance, cooling effect and regeneration temperature. Crum et al. [10] discussed more types of advanced cycles. These cycles were indirect evaporative cooling cycle and a cooling tower-heat exchanger combination cycle. Both cycles can be operated under ventilation of recirculation modes. Advanced cycles have significantly higher thermal coefficients of performance than the conventional system that employs only direct evaporative coolers. Joudi and Madhi [11] investigated experimentally

the performance of a solar assisted open adsorption cooling system. They concluded that the system performance improved with higher regeneration temperature, high process air mass flow rate and dry weather. Also, they found it is possible to generate a cool supply of air at satisfactory conditions for building cooling using only solar energy for all clear days under the weather conditions of Basrah.

Solar heating and cooling systems require collector arrays which may be connected in parallel, in series or in a combination of both. Series connection gives the temperature required for air conditioning purposes, while the parallel connection determines the required air flow rate. Oonk et al. [12] derived the mathematical modeling for calculating the performance of multi-collectors in series from test data on a single collector. It was possible to calculate the required slope and intercept for a collector array directly, knowing the slope and intercept data at the proper mass flow of a single collector. Duffie and Beckman [13] stated that two situations arise in which data from tests on single collector modules must be modified before they are applied to arrays. First, it may be desirable to put the collectors in series that are not identical (e.g., the first having one cover and the second having two covers). Second, if like collectors are arranged in series with the same flow velocity through the modules as in the test, the performance of the second module will be different from that of the first, as the inlet temperature to the second will be the outlet temperature from the first.

The use of many collector rows with limited spacing will increase the gross collector area but will also increase the shading effect. Therefore, it is important to determine accurately the reduction in net radiation flux due to collector shading. Appelbaum and Bany [14] developed an analytical–numerical shading model for rows of non-concentrating collectors tilted towards the equator. They also accounted for the beam radiation shadowing by considering the shaded area on a collector. They attempted to approximate the shading of diffuse radiation, but an error was introduced in their model. Jones and Burkhart [15] presented a totally analytical model for calculating the daily total radiation on rows of fixed collectors tilted toward the equator. A shading plane concept was adopted in their model. Bany and Appelbaum [16] derived a general expression for the shading and insolation of a field of solar collectors. The shading on a collector may be cast by its neighbor and/or by a fence and is dependent on the spacing between collector rows and on collector height, row length tilt angle and latitude location. The equations for the shadow height, length and area were given in dimensionless form and were, therefore, general relations. Also, the derivation pertained to collectors arranged in rows in the horizontal plane or raised in a step-like structure. It was deduced that the most critical parameter in collector shading was the spacing between the collectors, while the row length had a small effect on shading. Increasing the collector tilt angle causes the shadowing to increase.

The present work attempts to study a combined heating and desiccant cooling solar system through a systematic computer simulation of the system components. The heating load of a two story residence was calculated by the variable base degree day (VBDD) method and the cooling load by the transfer function method (TFM). Series and parallel connections of the solar array were analyzed together with the shading effect of collector rows. System performance was analyzed by the *f*-chart method and an evaluation of the system components was performed under various operating conditions. The solar air heater were used for winter heating and for desiccant regeneration in the summer.

2. Space heating and cooling loads

2.1. Estimation of heating load by variable base degree day method

Estimation of the heating load by the (VBDD) method requires an understanding of the concept of free energy which is the energy required for raising the base temperature to the indoor comfort condition (22°C) as:

$$Q_{\mathrm{f}} = \mathrm{UA}(T_{\mathrm{sp}} - T_{\mathrm{b}}) \tag{1}$$

Therefore, the base temperature is given as:

$$T_{\mathrm{b}} = T_{\mathrm{sp}} - \frac{Q_{\mathrm{f}}}{\mathrm{UA}} \tag{2}$$

and the heating load is:

$$Q_{\mathrm{L}} = \mathrm{UA}(T_{\mathrm{sp}} - T_{\mathrm{a}}) - Q_{\mathrm{f}} \tag{3}$$

Substitution of Eq. (1) gives:

$$Q_{\mathrm{L}} = \mathrm{UA}(T_{\mathrm{sp}} - T_{\mathrm{a}}) - \mathrm{UA}(T_{\mathrm{sp}} - T_{\mathrm{b}}) \tag{4}$$

Thus,

$$Q_{\mathrm{L}} = \mathrm{UA}(T_{\mathrm{b}} - T_{\mathrm{a}}) \tag{5}$$

The above equation calculates the heating load due to the exterior roof, walls, windows and doors. For an unheated floor slab Ref. [17] indicates that the heat loss from a concrete floor slab is more proportional to the perimeter than to the area of the floor and is found as:

$$Q_{\mathrm{floor}} = F_{\mathrm{e}} P_{\mathrm{f}} (T_{\mathrm{b}} - T_{\mathrm{a}}) \tag{6}$$

The infiltration heat loss is:

$$Q_{\mathrm{inf}} = \rho C_{\mathrm{p}} N_{\mathrm{ch}} V (T_{\mathrm{b}} - T_{\mathrm{a}})/3600 \tag{7}$$

The space free energy is composed of internal energy gains and solar gains as:

$$Q_{\mathrm{f}} = Q_{\mathrm{occ}} + Q_{\mathrm{lig}} + Q_{\mathrm{sol}} + Q_{\mathrm{op}} \tag{8}$$

where Q_{occ} and Q_{lig} are obtained from the schedules of occupancy and lighting as shown in Table 1.

Solar gain through windows is given by [17]:

$$Q_{\mathrm{sol}} = S_{\mathrm{c}} \cdot \mathrm{SHGF} \cdot A_{\mathrm{rw}} \tag{9}$$

and the solar heat gain through opaque surfaces is:

Table 1
A 24 h schedule for the lighting and occupation sensible heat gains (W)[a]

Local time	Lights	Occupants	Local time	Lights	Occupants
1	210	390	13	430	260
2	210	390	14	430	390
3	210	390	15	430	390
4	210	390	16	430	390
5	210	390	17	430	390
6	210	390	18	2600	390
7	430	390	19	2600	390
8	430	390	20	2600	390
9	430	130	21	2600	390
10	430	130	22	2600	390
11	430	130	23	2600	390
12	430	130	24	2600	390

[a] Numbers of persons is five.

$$Q_{op} = (UA)_s \left(\frac{\alpha_0}{h_0}(I_T) - \frac{\varepsilon_s \Delta R}{h_0} \right) \tag{10}$$

2.2. Calculation of cooling load by transfer function method

Calculation of the heat flow through exterior walls and roofs can be achieved using the sol–air temperature, which is given as [17]:

$$T_{sol} = T_a + \frac{\alpha_0}{h_0} I_T - \frac{\varepsilon_s \Delta R}{h_0} \tag{11}$$

The hour by hour calculation of heat gains using the TFM is given as [17]:

$$\frac{q_\tau}{A_r} = \sum_{n=0} (b_n T_{sol,\tau - n\Delta}) - \sum_{n=1} \left(d_n \frac{q_{\tau - n\Delta}}{A_r} \right) - T_{sp} \left(\sum_{n=0} C_n \right) \tag{12}$$

The transfer function coefficients b_n, d_n and C_n, as well as U values are tabulated for different roofs and walls constructions by ASHRAE [17].

The calculation procedure of the heat gain at a given time requires information on the sol–air temperature at that time and preceding times in addition to the heat gain at previous times. For example, if the heat gain at the first hour is calculated, the preceding values of sol–air temperature are unknown but are taken from the 24 h cycle of the sol–air temperature as:

$$T_{sol(0)} = T_{sol(24)} \tag{13}$$

$$T_{sol(-1)} = T_{sol(23),} \text{ etc.} \tag{14}$$

but the preceding values of heat gain are unknown, therefore, for the initial calculation, they are assumed to be zero. The effect of this assumption on the calculated heat flow values becomes negligible as the calculation is repeated for successive 24 h cycles.

To offset the effect of the above initial starting value, two ways are indicated. The first is by the convergence between the heat gain values to a periodic steady state condition. This is indicated by comparing the average of the last 24 values with the average heat flow (the product of U value and the difference between the average sol–air temperature and inside space temperature) [17]:

$$q_{\mathrm{av}} = U(\overline{T}_{\mathrm{sol}} - T_{\mathrm{sp}}) \tag{15}$$

The second way is by repeating the solution for the M cycles of time and noting the heat gain values for the cycle $M-1$ and the last cycle M. If these values are approximately identical then the values of heat gain of the last cycle are taken to estimate the cooling load. Otherwise, the number of cycles M is increased. Demonstration of this technique is done by noting the convergence of four cycles for the heat gain values of the south wall as shown in Table 2. This procedure is adopted in the present work to calculate the heat gain.

The corresponding cooling load Q_τ at time τ can be related to the current value of heat gain q_τ and the preceding values of cooling load and heat gain as [17]:

$$Q_\tau = (v_0 q_\tau + v_1 q_{\tau-\Delta} + v_2 q_{\tau-2\Delta} + \cdots) - (w_1 Q_{\tau-\Delta} + w_2 Q_{\tau-2\Delta} + \cdots) \tag{16}$$

In general, the TFM coefficients, vs and ws, depend on the size of time element Δ, the nature of the heat gain and the storage capacity of the space. These coefficients are listed in Ref. [17].

Table 2
Convergence of heat gain values, (W) for four cycles

$M=1$	$M=2$	$M=3$	$M=4$
158.2353	1771.071	1774.53	1774.536
298.857	1563.303	1565.979	1565.983
389.09	1371.273	1373.343	1373.346
431.5034	1192.218	1193.819	1193.822
438.1795	1026.824	1028.062	1028.064
420.7288	876.0912	877.0489	877.0506
395.7553	747.9812	748.722	748.7233
416.7838	689.2249	689.7979	689.7988
513.8134	742.5403	742.9835	742.9842
747.2827	910.3746	910.7174	910.718
1064.736	1190.806	1191.071	1191.072
1466.082	1563.594	1563.799	1563.799
1914.464	1989.887	1990.045	1990.046
2347.607	2405.944	2406.067	2406.067
2703.795	2748.918	2749.013	2749.013
2958.101	2993.003	2993.076	2993.076
3091.915	3118.91	3118.967	3118.967
3114.6	3135.48	3135.524	3135.524
3060.927	3077.077	3077.11	3077.11
2933.589	2946.082	2946.108	2946.108
2736.948	2746.611	2746.631	2746.631
2496.086	2503.56	2503.575	2503.575
2239.981	2245.762	2245.774	2245.774
1996.331	2000.802	2000.811	2000.8111

The calculation of the cooling load at a given time requires information of the heat gain at that and preceding times in addition to the cooling load at previous times. All unknown values of cooling load are assumed to be zero for the initial calculation. Therefore, the M cycle procedure is taken to evaluate the cooling load.

The cooling load due to exterior windows is calculated by:

$$Q_\tau = (v_0 \mathrm{SHG}_\tau + v_1 \mathrm{SHG}_{\tau-\Delta} + \cdots) - (w_1 Q_{\tau-\Delta} + w_2 Q_{\tau-2\Delta} + \cdots) \tag{17}$$

The solar heat gain is given as:

$$\mathrm{SHG} = S_c \cdot \mathrm{SHGF} \tag{18}$$

The cooling load due to lighting is given by Eq. (16) with $v_0 = 0$ (i.e. the cooling load due to lighting at time τ is not related to the heat gain at the same time).

The sensible cooling load due to occupants and infiltration air takes the same values of the corresponding heat gain because they include only the convective portion.

3. Collector arrays model

Collector modules in arrays may be connected in parallel, in series or in a combination of both. Because of the large number of possible array configurations, it is unreasonable to expect measured test data for all possible array arrangements. Therefore, the performance of collectors in series can be obtained from test data on a single collector.

The array in the present work is composed of air heating, single cover collectors. The absorber plate is V corrugated with a 60° angle of corrugation. Each collector measured $1.2 \times 2.8\ \mathrm{m}^2$ on the outside dimensions with an aperture area of $2.7\ \mathrm{m}^2$. This is the same type of collector used in the experimental investigation of Joudi and Madhi [11].

For M identical collectors in series, Oonk et al. [12] derived the following equations for the intercept and slope of the efficiency curve:

$$[F_R(\tau\alpha)]_M = \mathrm{CFM} F_{R1}(\tau\alpha)_1 \tag{19}$$

$$[F_R(U_L)]_M = \mathrm{CFM} F_{R1}(U_{L1}) \tag{20}$$

and

$$\mathrm{CFM} = \frac{1}{MZ}[1 - (1 - Z)^M] \tag{21}$$

where

$$Z = \frac{A_1 F_{R1} U_{L1}}{\dot{m} C_p} \tag{22}$$

A collector may be shaded by its neighboring collector and/or by a fence. Fig. 1 describes two collectors and the shadow cast by the first collector on the second.

The derivations of shadow height and length are given by Bany and Appelbaum [14]. The relative shadow height and length are:

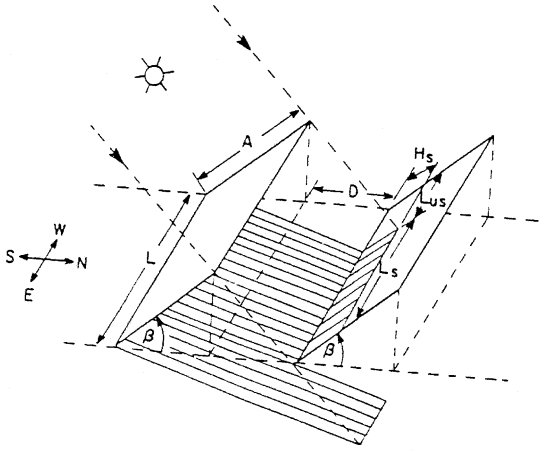

Fig. 1. Collector shading model.

$$h_s = \frac{H_s}{A} = 1 - \frac{d\sin\beta + \cos\beta}{\cos\beta + \sin\beta\cos\gamma_s/\tan\alpha} \tag{23}$$

$$\ell_s = \frac{L_s}{L} = 1 - \left(\frac{|\sin\gamma_s|}{1\tan\alpha}\right)\left(\frac{d\sin\beta + \cos\beta}{\cos\beta + \sin\beta\cos\gamma_s/\tan\alpha}\right) \tag{24}$$

where

$$d = \frac{D}{H_c} \tag{25}$$

$$\ell = \frac{L}{H_c} \tag{26}$$

and

$$H_c = A\sin\beta \tag{27}$$

The relative shadow area is then:

$$r_s = \frac{H_s L_s}{AL} = h_s \ell_s \tag{28}$$

and $r_s \geqslant 0$ for non-negative values of both h_s and ℓ_s, otherwise $r_s = 0$.

The effect of shading is reflected in the calculations of both beam and diffuse irradiance as:

$$I_{bs} = I_{DN}\cos\theta(1 - r_s) \tag{29}$$

$$I_{ds} = I_{DN}\left[C\frac{1+\cos\beta}{2} + \rho_g(C + \sin\alpha)\frac{1-\cos\beta}{2} - \frac{1}{2}\left(\left(d^2+1\right)^{1/2} - d\right)\sin\beta\right] \tag{30}$$

and the total irradiance on a shaded collector is the sum of both beam and diffuse irradiance as:

$$I_{TS} = I_{bs} + I_{ds} \tag{31}$$

4. Prediction of solar air heating system performance

The present solar heating system shown in Fig. 2 is approximately similar to the standard system. Therefore, the *f*-chart method is an efficient means for estimating the fraction of total heating load that will by supplied by solar energy.

The monthly fraction is related to two dimensionless groups, one associated with the ratio of collector losses to heating load X and the second related to the ratio of absorbed energy to heating load Y, as [2]:

$$X = AF_R U_L (T_{ref} - \overline{T}_a)\,\Delta t / L_T \tag{32}$$

$$Y = AF_R(\overline{\tau\alpha})\overline{I}_T N / L_T \tag{33}$$

Then, the correlation of solar fraction is given as:

$$f = 1.04Y - 0.065X - 0.159Y^2 + 0.0018X^2 - 0.0095Y^3 \tag{34}$$

The monthly total heating load can be written as

$$L_T = \mathrm{UA}(\overline{T}_b - \overline{T}_a)\Delta t \tag{35}$$

The average base temperature for each month is found as:

$$\overline{T}_b = \frac{\sum T_b}{24} \tag{36}$$

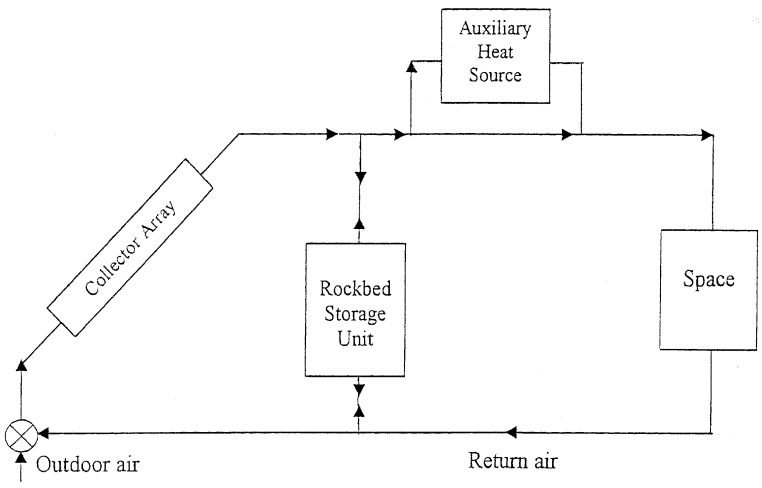

Fig. 2. Schematic diagram of the simulated solar air heating system.

The effects of changes in collector air flow rate and storage capacity of the packed bed must be considered, respectively, as:

$$\frac{X_c}{X} = \left(\frac{\dot{m}_f}{10.1}\right)^{0.28} \quad \text{for } 5 < \dot{m}_f < 20 \tag{37}$$

$$\frac{X_c}{X} = \left(\frac{V_s}{0.25}\right)^{-0.3} \quad \text{for } 0.125 < V_s < 1 \tag{38}$$

5. Desiccant cooling system

The solar assisted desiccant cooling system is shown in Fig. 3. The regenerative dehumidifier model uses simplified non-linear combined potential functions of air temperature and humidity ratio as [9]:

$$F_1 = \frac{-2865}{T^{1.49}} + 4.344W^{0.8624} \tag{39}$$

$$F_2 = \frac{T^{1.49}}{6360} - 1.127W^{0.07969} \tag{40}$$

The above combined potentials for the inlet conditions of the process and the regeneration air streams can be easily estimated. The combined potentials for the outlet process air stream are then attained from the following regenerative dehumidifier efficiencies as [9]:

$$F_{1p,o} = \eta_{F_1}(F_{1r,i} - F_{1p,i}) + F_{1p,i} \tag{41}$$

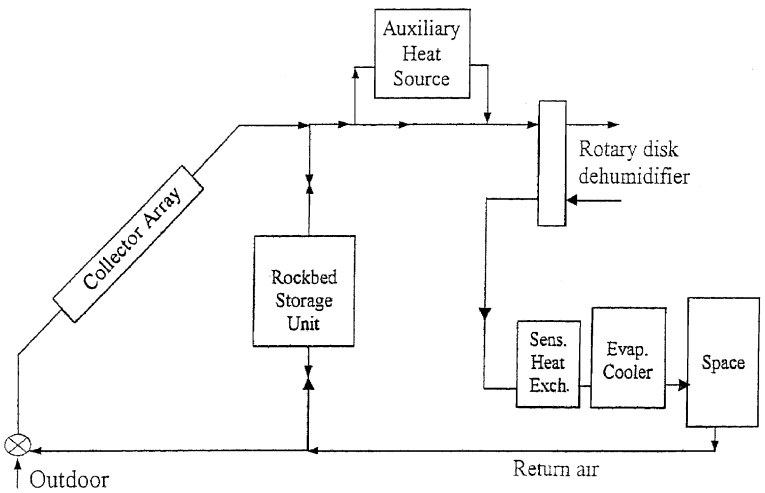

Fig. 3. Schematic diagram of the simulated solar desiccant cooling system.

$$F_{2p,o} = \eta_{F_2}(F_{2r,i} - F_{2p,i}) + F_{2p,i} \tag{42}$$

where η_{F_1} and η_{F_2} represent the regenerative F_1 and F_2 potential efficiencies, respectively. It can be observed from these equations that low values of η_{F_1} (closer to 0) and high values of η_{F_2} (closer to 1) make the dehumidifier closer to the ideal state.

The outlet process air temperature and moisture content can be obtained by solving Eqs. (39) and (40) simultaneously with the combined potential calculated from Eqs. (41) and (42), respectively. Also, three pairs of (η_{F_1}, η_{F_2}) values were selected. They were (0.05,0.95), (0.08,0.8) and (0.1,0.7), referring to good (GDP), medium (MDP) and poor (PDP) dehumidifier performances, respectively [8].

The air is sensibly cooled by a water cooled cross flow heat exchanger. The outlet state of the process air from the heat exchanger can be evaluated as:

$$T_{p,o} = T_{p,i} + \eta_{hx}(T_{w,i} - T_{p,i}) \tag{43}$$

The temperature of cooled water entering the heat exchanger was assumed equal to 3°C greater than the ambient design wet bulb temperature. The reference value of heat exchanger effectiveness was taken at 0.85.

The dry bulb temperature of process air air leaving the evaporative cooler (supply temperature) is:

$$T_{e,o} = T_{e,i} + \eta_{ev}(T_{e,i} - T_{ew,i}) \tag{44}$$

The value of evaporative cooler effectiveness was taken at 0.8.

The performance of the desiccant cooling system is commonly expressed in terms of the coefficient of performance COP. The coefficient of performance is defined as the heat removed from the process air stream divided by the energy input to the cycle as [11]:

$$\mathrm{COP} = \frac{\dot{m}_p(h_a - h_{sup})}{\text{Energy input}} \tag{45}$$

The energy input to the cycle consists of electric energy to circulate the air and water and to rotate the desiccant wheel and the auxiliary energy required to regenerate the desiccant dehumidifier, which is calculated as:

$$\text{Auxiliary energy} = \dot{m}_{reg}C_p(T_{reg} - T_{out}) \tag{46}$$

while the solar energy is considered free.

6. Results and discussion

The details of the building construction considered in the present work are given in Appendix A.

6.1. Space heating and cooling load

Heating load calculation by the VBDD method depends on the free energy of the building. Therefore, the components of this energy will affect the profile of the heating load. Fig. 4 shows

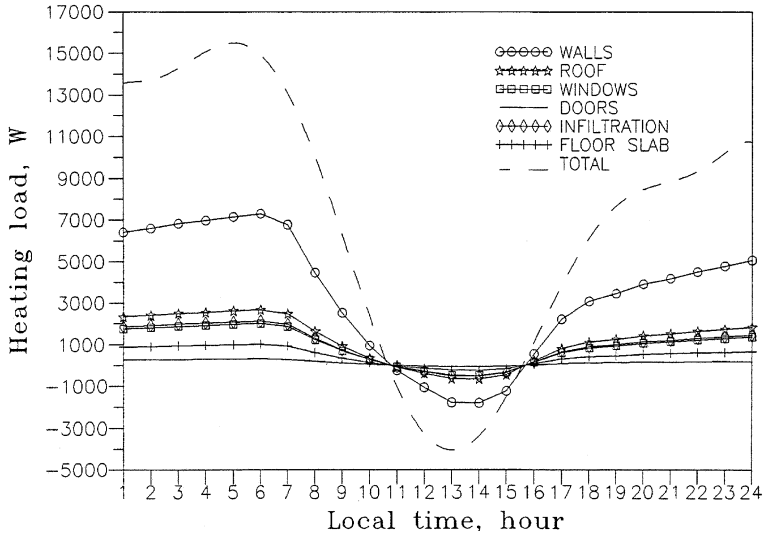

Fig. 4. Contribution of various heat load components to the total heating load in December.

the contribution of various heat load components and the total heating load in December. The total heating load is obtained by the sum of all the individual components. It is clear that the exterior walls constitute the major part of the heating load, while exterior doors have the minimum heating load. The comfort indoor space temperature is considered as constant at 22°C. For the period of no heating load from 11 a.m. to 4 p.m., the outlet air from the collector array is used for charging the rock bed storage unit.

Fig. 5 shows the hourly values of total heating load estimated by the VBDD and the traditional DD methods with a base temperature of 18.3°C. For the first 7 h of the day, the DD heating load

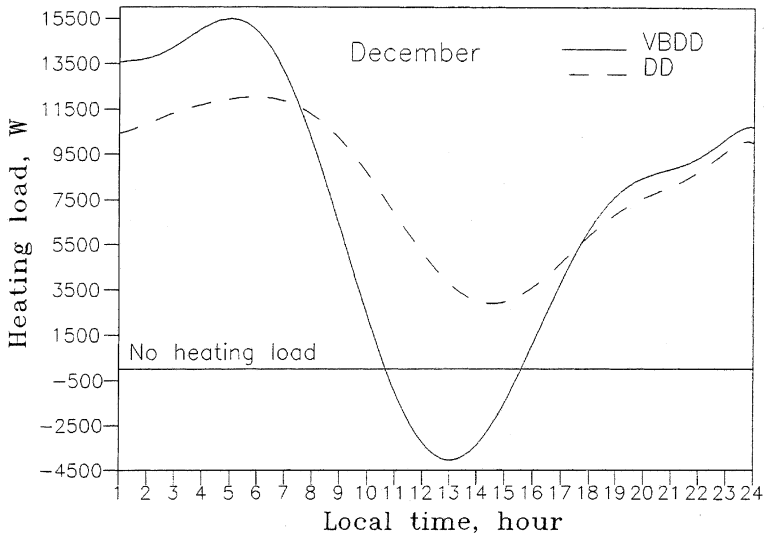

Fig. 5. Comparison between load estimated by variable and normal base DD methods.

is lower than that of the VBDD because the major part of free energy, which is solar radiation, is absent. Therefore, the base temperature of the VBDD is greater than 18.3°C. For the same reason, this trend is obtained for the last 7 h of the day. When the solar radiation effect appears, the VBDD heating load is lower than that of the DD. The average base temperatures were found as 17.5, 17.3 and 16.8°C for recommended days of December, January and February, respectively. The energy saved by using the VBDD method is about 4.2%, 5.46% and 8.36% for these months, respectively, as compared with the DD method. It is obvious that the peak heating load is associated with the minimum ambient temperature at 6 a.m.

A large number of variables are included in making up the cooling load due to the storage (transient) nature inherent within the cooling load. The hourly profile of total cooling load and its components is shown in Fig. 6. The sum of the cooling load components gives the total load of the building. The peak load of the building occurs at 6 p.m., and this value should be taken for design purposes, such as the determination of the number of collectors in parallel and series as shown in Appendix A. The percentage of the various components of the peak cooling load is shown in Fig. 7.

6.2. Collector array and shading effect

The performance of a collector array in a parallel fashion is obtained by knowing the performance of a single collector if the mass flux is the same in all collectors. The performance of a single collector should be modified to estimate the performance of collectors connected in series at the proper mass flow. In the present work, a combined parallel-series fashion is used. A shading effect occurs when collectors are connected in rows.

Fig. 8 depicts the hourly variation of the outlet air temperature for a hypothetical case of three collectors in series without a shading effect. It is noted that the temperature difference between the

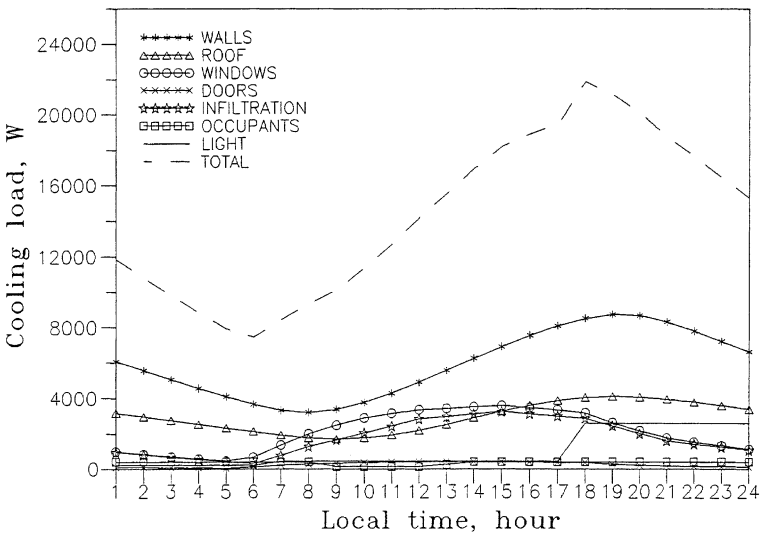

Fig. 6. Hourly variation of cooling load for various heat gain components in July.

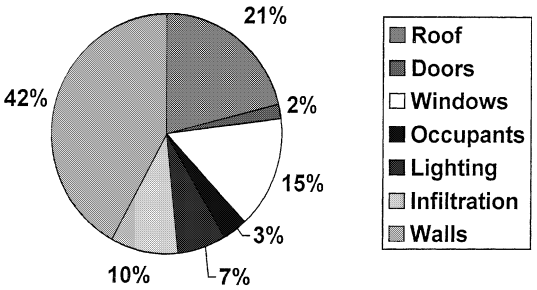

Fig. 7. Contribution of the various heat gain components to the peak sensible cooling load.

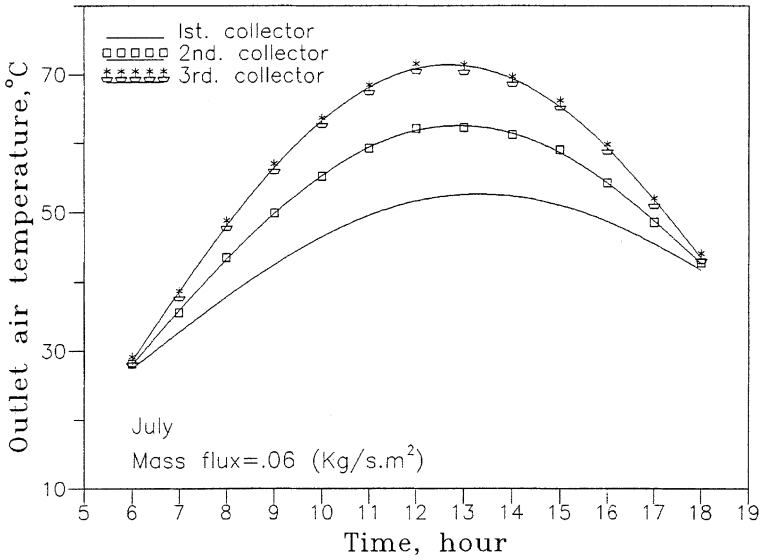

Fig. 8. Variation of outlet air temperature for three collectors in series.

first two collectors is higher than that between the second and third collectors. This behavior is usual because the heat loss from a collector increases as the inlet air temperature increases. Thus, for the same incident radiation on all collectors, the heat gain decreases, and the temperature difference between successive collectors decreases as well.

Fig. 9 shows the instantaneous collection efficiency variation of three collectors in series. The variation in the value of collection efficiency from 9 a.m. to 3 p.m. is small. This is mainly due to the combined effect of the fraction of absorbed solar radiation and thermal losses from the collector during the day.

Fig. 10 shows the hourly variation of outlet air temperature for two collectors in series for different air mass fluxes. It is obvious that when the air flow rate increases, the outlet air temperature from two collectors in series decreases. The variation in outlet air temperature by changing the mass flux from 0.02 to 0.04 kg/s m^2 of collector area is greater than that from 0.04 to 0.06 kg/s m^2 of collector area. This is because the useful energy gain varies proportionally with the

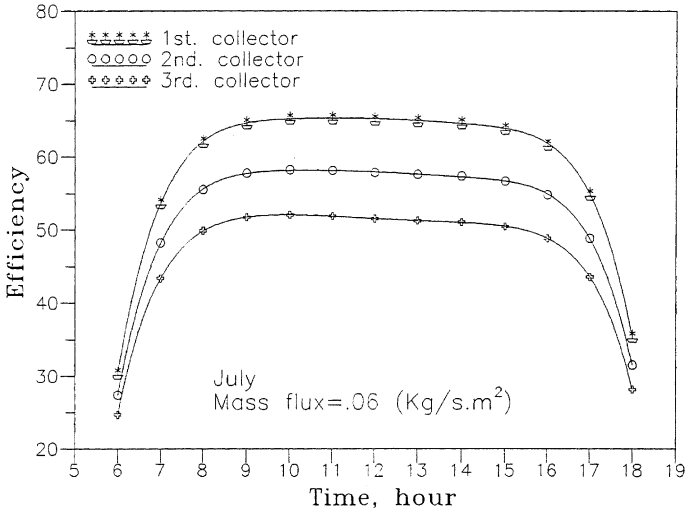

Fig. 9. Efficiency variation of three collectors in series.

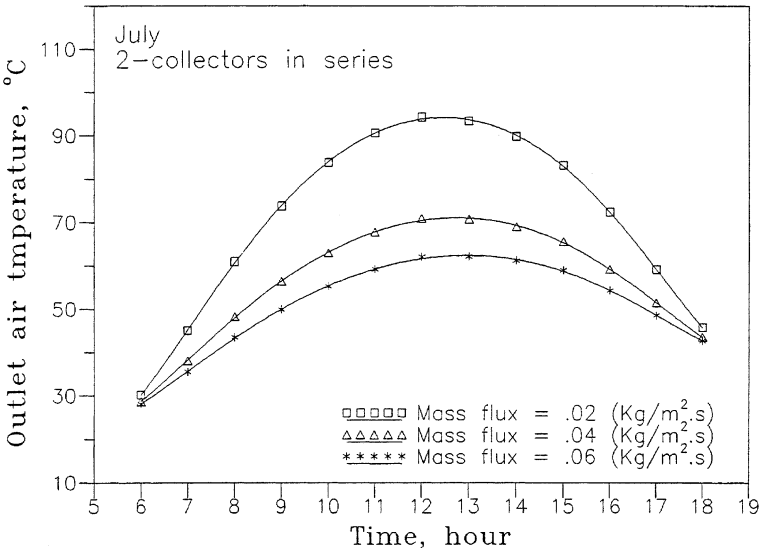

Fig. 10. Variation of outlet air temperature for various air mass flux.

air flow rate, but for high air flow rate, the improvement in the energy gain becomes smaller due to larger thermal losses. Increasing the mass flux 0.02 to 0.06 kg/s m^2 of collector area results in a maximum reduction in outlet air temperature (from 95°C to 62°C) of about 35% at midday.

The shading effect is highly dependent on the tilt angle and collector spacing. Fig. 11 shows the hourly variation of total radiation received by the collector for different ratios of row spacing to collector width (Fig. 1). The results prove that the shading effect is nearly negligible for spacing to collector width ratios of 1.5, 2 and 2.5.

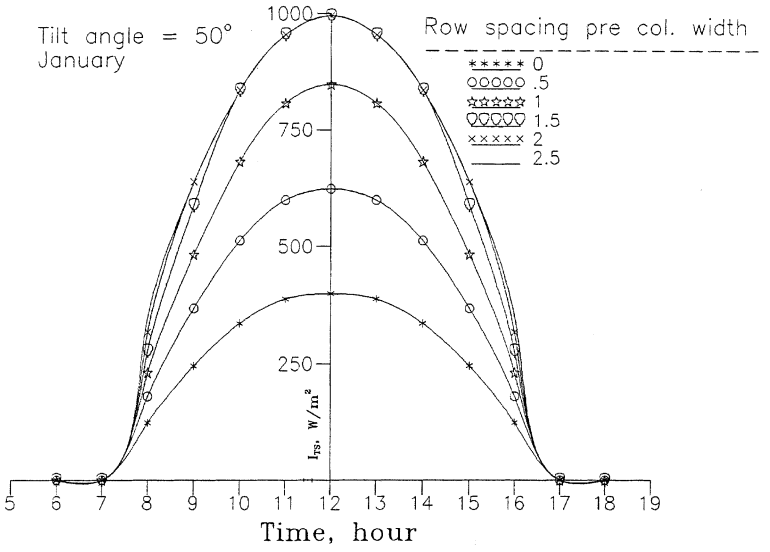

Fig. 11. Effect of distance between collectors on the total incident irradiance.

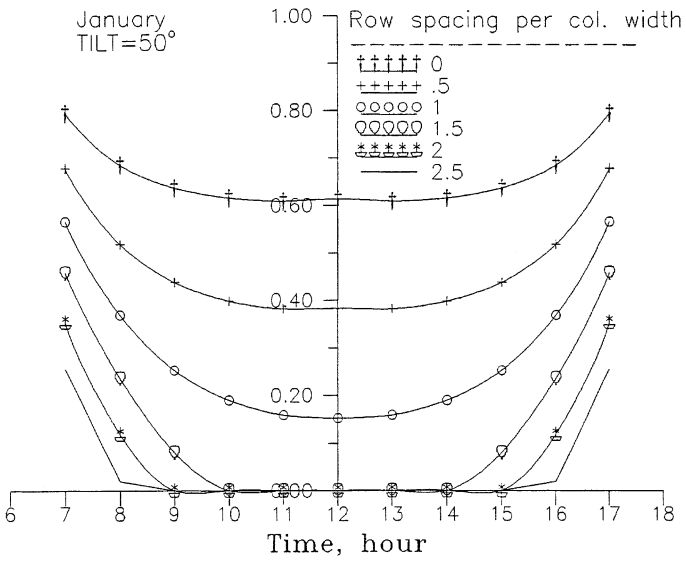

Fig. 12. Hourly variation of relative shaded area in January.

Fig. 12 describes the hourly variation of relative shaded area for different ratios of row spacing to collector width. The relative shaded area is symmetrical about 12 noon. The relative shaded area decreases in the morning hours up to noon because the incidence angle decreases. Also, it is seen that there is no shading effect (relative shaded area equals zero) from 10 a.m. to 2 p.m. for the

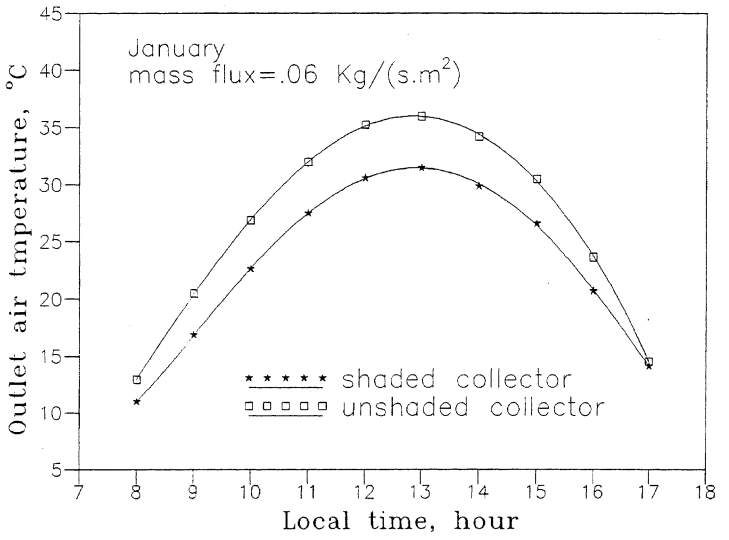

Fig. 13. Effect of shading on outlet air temperature for two collectors in series.

spacing to width ratios of 1.5, 2 and 2.5. The results of Figs. 11 and 12 are in good agreement with that of Ref. [16].

Fig. 13 shows the effect of shading on the outlet air temperature from the second collector for two collectors in series spaced 2 m apart. The useful heat gain of a shaded collector is lower than that of the unshaded collector. Therefore, its outlet air temperature is lower too. At 1 p.m., the outlet air temperature from the unshaded collector (36°C) is about 16% greater than that from the shaded collector (31°C) for an air mass flux of 0.06 kg/s m^2 of collector area in January.

Fig. 14 shows the variation of outlet air temperature for two collectors in series for an air mass flux of 0.06 kg/s m^2 of collector area with the presence of shading effect. The maximum outlet temperature from this collector array is about 31°C, which is very suitable for a supply air temperature in the winter season. By reducing the air mass flux, the outlet air temperature can be increased. For periods when the outlet air temperature is above the required supply air temperature, it is used for charging the rock bed storage unit. For the periods when the required supply temperature is not achieved by the solar collector array, the air is directed to the auxiliary heat source to obtain the required temperature.

6.3. Solar heating system performance

The performance prediction of the solar air heating system is obtained by the *f*-chart method. The load fraction supplied by solar energy is evaluated for different design variables, such as collector area, air flow rate and rock bed storage volume.

Fig. 15 depicts the variation of the monthly solar fraction with the area of collectors. It is clear that increasing the collector area over an optimum value will lead to only low improvements in solar fraction. This is very obvious in December as the optimum collector area is 54 m^2.

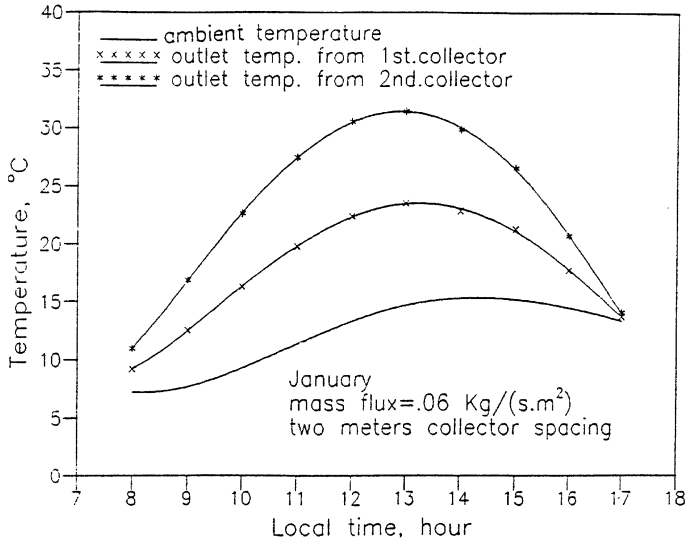

Fig. 14. Variations of outlet air temperature for two collectors in series with shading effect.

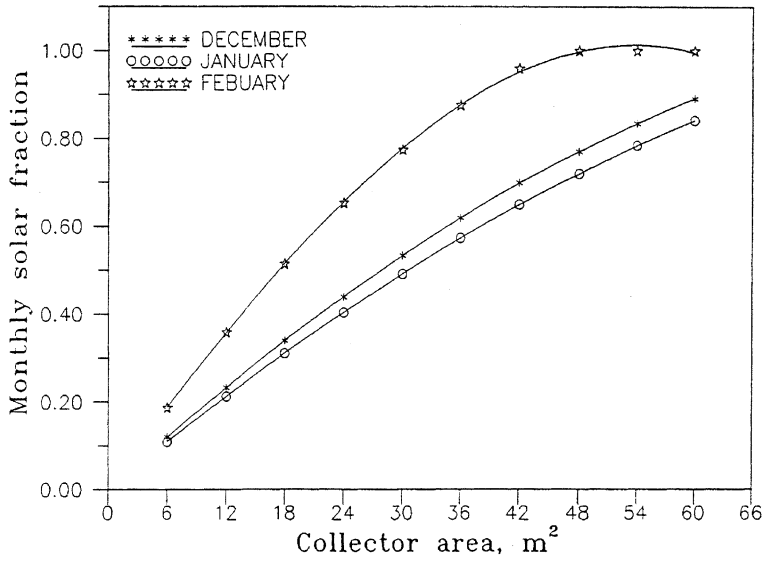

Fig. 15. Variation of solar fraction with area of collector array.

Fig. 16 shows the effect of air mass flux through the collectors on the monthly heating load that will be met by solar energy for December and January with a collector area of 54 m^2. It is evident that this effect is rather small, and these results are in very good agreement with those of Refs. [2,13]. A change of air mass flux from 10 to 20 l/s m^2 of collector area only causes a 2.8% increase in monthly solar fraction in December. An increase in air flow rate tends to improve system performance by increasing the value of the heat removal factor, but it also tends to decrease

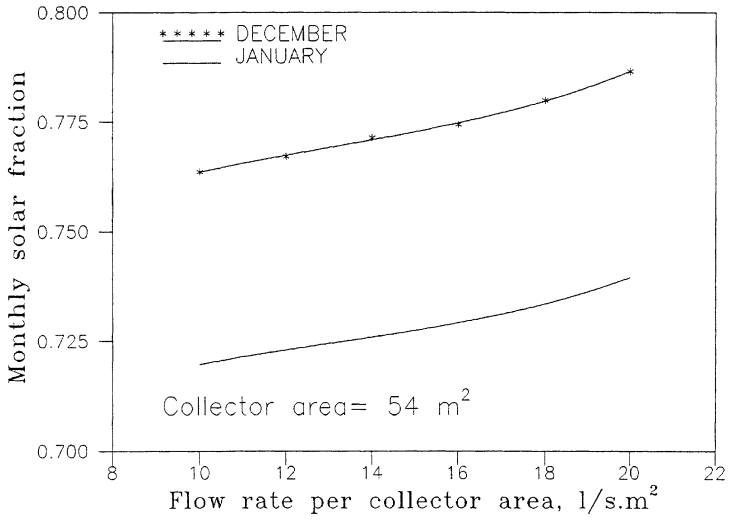

Fig. 16. Variation of solar fraction with air mass flux.

performance somewhat by reducing the degree of thermal stratification through the rock bed storage unit.

The performance of an air heating system is less sensible to storage capacity than that of a liquid system, as shown in Fig. 17. A change of storage capacity from 0.125 to 1 m^3 of rocks per square meter of collector area causes an increase in monthly solar fraction of only 15%, 14.7% and

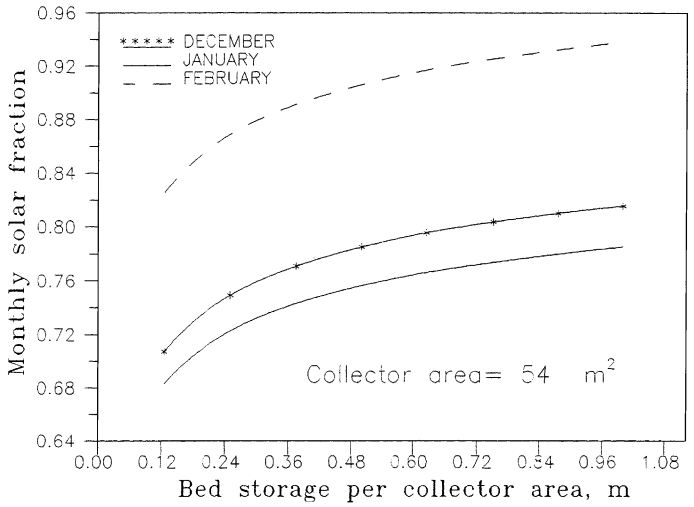

Fig. 17. Variation of solar fraction with bed storage volume.

15.3% in December, January and February, respectively, for a collector array area of 54 m^2. This is in agreement with the results of Refs. [2,13].

6.4. Desiccant cooling system performance

The influence of various designs and operating conditions on the performance of the open cycle desiccant cooling system is examined using the developed simulation technique. These conditions consist of ambient temperature, ambient moisture content, regeneration temperature, evaporative cooler effectiveness, heat exchanger effectiveness and dehumidifier effectiveness. The performance of the desiccant cooling system is evaluated in terms of supply air temperature and system coefficient of performance. The system operates under the ventilation mode.

Fig. 18 shows the reduction of moisture content with regeneration temperature for constant values of inlet (ambient) temperature and inlet moisture content and for various dehumidifier performances. As the regeneration temperature increases, the adsorption capacity of the silica gel is increased. Therefore, the silica gel becomes capable of adsorbing larger amounts of water vapor.

Fig. 19 shows the effect of regeneration temperature on the supply air temperature for constant values of inlet (ambient) moisture content and temperature of the process air stream. As the regeneration temperature increases from 50°C to 95°C, the reduction in supply air temperature is 12.5%, 10% and 9% for GDP, MDP and PDP, respectively. This is because an increase in regeneration temperature increases the outlet process air temperature, but the outlet process air moisture is decreased. Therefore, the process air enters the evaporative cooler at a lower wet bulb temperature, meaning that the final supply air temperature will be lower.

The variation of coefficient of performance with the heat exchanger and evaporative cooler effectivenesses is shown in Fig. 20. As the effectiveness of the heat exchanger or evaporative cooler increases, the supply air temperature decreases. Therefore, and according to Eq. (45), the coef-

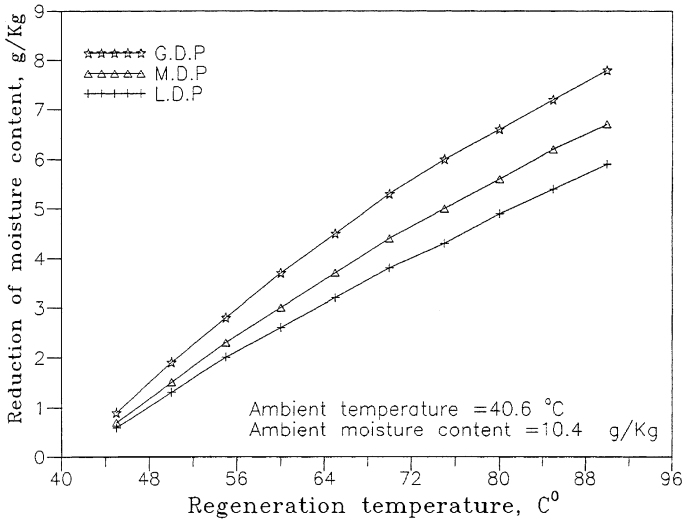

Fig. 18. Effect of regeneration temperature on the reduction of moisture content.

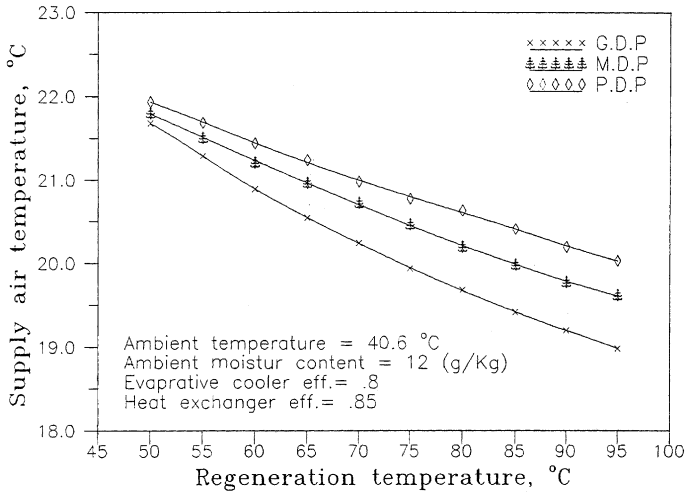

Fig. 19. Variation of supply temperature with regeneration temperature.

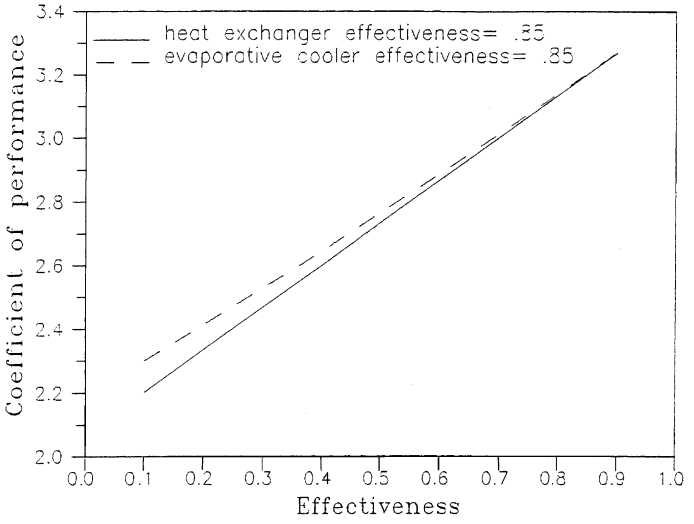

Fig. 20. Effect of sensible and evaporative coolers effectiveness on the coefficient of performance.

ficient of performance increases. Changing the heat exchanger and evaporative cooler effectivenesses from 0.1 to 0.9 causes an increases in coefficient of performance by 41.3% and 47.7%, respectively.

Fig. 21 shows the effect of regeneration temperature on the coefficient of performance at 12 noon in July. It is known that the regeneration of a desiccant bed requires the combination of collector array and auxiliary heat source. The regeneration temperature of 62°C can be achieved by the collector array alone. For this reason, the value of the coefficient of performance did not change when the regeneration temperature changed from 56°C to 62°C because solar energy is

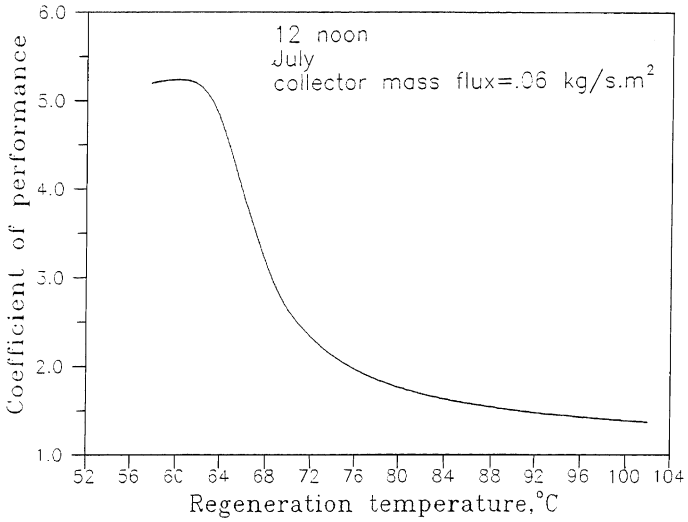

Fig. 21. Variation of coefficient of performance with the regeneration temperature.

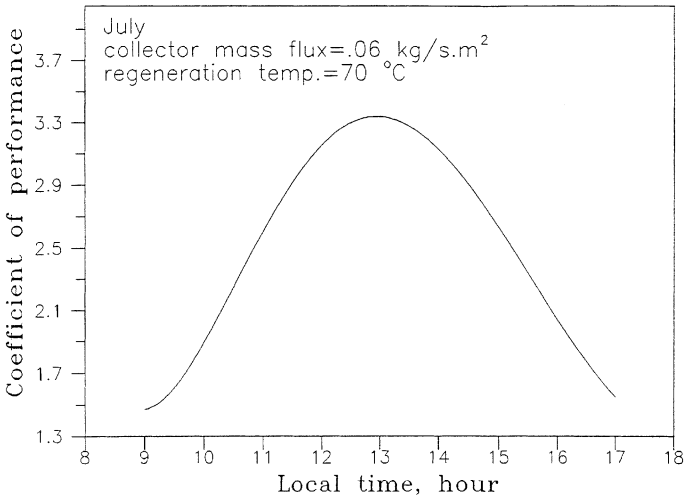

Fig. 22. Hourly variation of coefficient of performance.

considered free. As the regeneration temperature increases, the auxiliary heat source is used, causing an increase in the energy input to the system, and therefore, the coefficient of performance starts decreasing. At higher regeneration temperatures, the reduction in coefficient of performance becomes slow due to the auxiliary energy being relatively very high compared with the heat removed from the process air.

The hourly variation of coefficient of performance is indicated in Fig. 22 for a constant regeneration temperature of 70°C and air mass flux through the collector array of 0.06 kg/s m^2. The

maximum coefficient of performance takes place at 1 p.m. This variation is mainly due to the variation of ambient conditions. The coefficient of performance is averaged for the period of maximum solar heat collection from 10 a.m. to 4 p.m. to get the value of the coefficient of performance in July as 2.64. This result is in very good agreement with the experimental results achieved by Joudi and Madhi [11].

7. Conclusions

(1) The VBDD method is more accurate than the traditional DD method because it depends on hourly calculation of solar radiation and interior heat sources.

(2) Increasing the number of collectors in series causes a reduction in performance of the collector array. Therefore, two collector rows are used, giving an air temperature of 36°C and 62°C at midday in January and July, respectively, at a mass flux of 0.06 kg/s m^2.

(3) The minimum acceptable distance between rows for 2.8 m collectors tilted at 50° for Baghdad in the winter season is 4.2 m.

(4) The effect of air mass flow rate on the monthly solar fraction is not significant. Also, increasing the rock bed storage volume produces only a small improvement in the solar fraction.

(5) The desiccant cooling system can supply air at satisfactory comfort conditions in summer under the local weather of Baghdad.

(6) The performance of the desiccant cooling system is greatly influenced by the effectivenesses of the heat exchanger and the evaporative cooler and also by the regeneration temperature, while the effect of dehumidifier performance is relatively small.

Appendix A. The building under study and solar system design

The domestic building in the present work is a two story dwelling as shown in Fig. 23, located in Baghdad (latitude is 33.3°N and longitude is 44.4°E). The construction of the exterior roofs, walls, windows and doors are given in Tables 3 and 4. The design of the collector array depends on the peak seasonal load, which is the peak cooling load, while the profile of the heating load determines the periods where heated air from the collector array is supplied to the conditioned space or/and used for charging the rock bed storage unit.

Determination of the number of collectors is done by the following procedure:

The peak cooling load is about 22 kW as shown in Fig. 6. The roof mounted collectors reduce the load due to shading, but not all of it is eliminated. The roof load is 21% of the total cooling load (Fig. 7). The actual maximum cooling load becomes approximately 18 kW. A supply air temperature of 19.5°C was obtained with a GDP desiccant cooling system at a regeneration temperature of 84°C as shown in Fig. 19. Thus, the supply (process) air flow rate is given by:

$$\dot{m}_p = \frac{\text{Peak load}}{C_p(T_{sp} - T_{sup})} = \frac{18}{1.026(25 - 19.5)} = 3.1 \text{ kg/s}$$

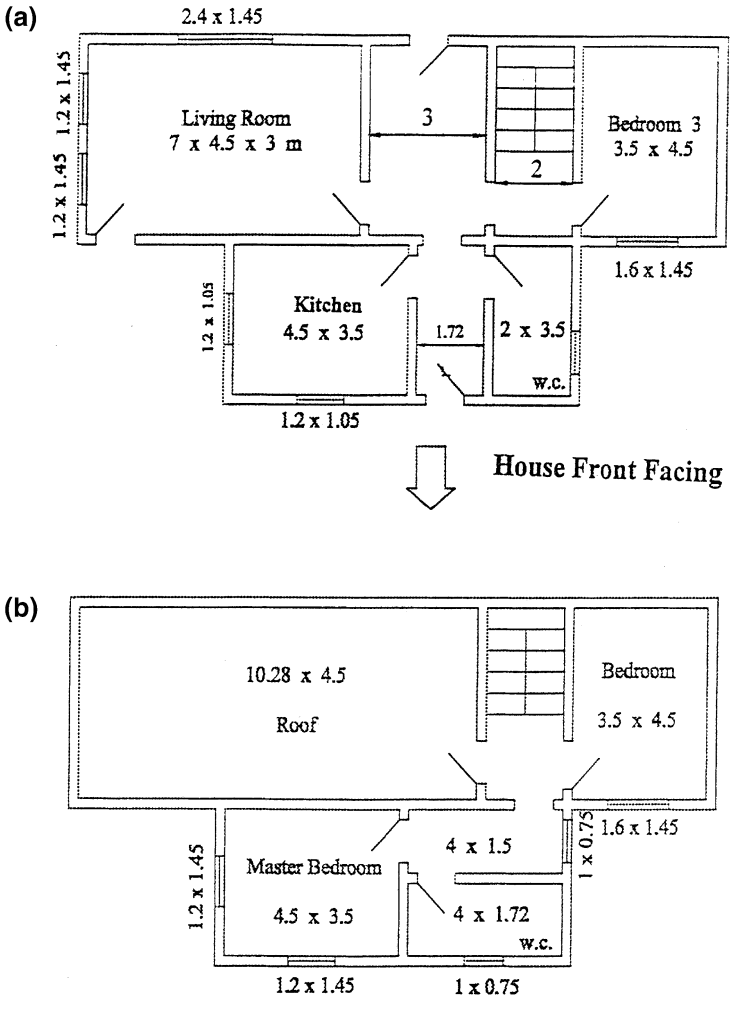

Fig. 23. House plan (a) ground floor, (b) first floor.

The ratio of regeneration to process air flow rate used in this work was selected at 2:3 or 0.66, hence,

$$\dot{m}_{\mathrm{reg}} = 0.66\ \dot{m}_{\mathrm{p}} \approx 2\ \mathrm{kg/s}$$

Let the mass flux through each collector be 0.06 kg/s m^2 with a collector area of 2.7 m^2. Therefore, the air mass flow rate through a collector is:

$$\dot{m}_{\mathrm{c}} = 0.06(2.7) = 0.162\ \mathrm{kg/s}$$

The number of collectors in parallel can be found as:

$$M_{\mathrm{p}} = \frac{\dot{m}_{\mathrm{reg}}}{\dot{m}_{\mathrm{c}}} = \frac{2}{0.162} \approx 12\ \text{collectors.}$$

Table 3
Building materials employed in the domestic building

Description		Density (kg/m^3)	Thickness (mm)	Thermal conductivity (W/m °C)	Thermal resistance (m^2 °C/W)
i_H	Inside horizontal surface resistance	–	–	–	0.1631
i_V	Inside vertical surface resistance	–	–	–	0.1206
0	Outside surface resistance[a]	–	–	–	0.0441
1	Heavy weight concrete	2243	150	1.731	0.0866
2	Common brick	1920	240	0.72	0.3333
3	Roof concrete tiles	–	40	0.852	0.0469
4	Sand	1500	75	0.33	0.2273
5	Cement plaster	1860	15	0.721	0.0208
6	Gypsum plaster	1680	10	0.81	0.0123
7	Juss plaster	1858	15	0.692	0.0216
8	Felt	–	–	–	0.0102
9	Asphalt	–	6	0.75	0.008
10	Glass	–	4	0.78	0.0051
11	Wood	593	50	0.159	0.3144
12	Steel	7689	2	44.998	0.00004
13	Styropore	30	50	0.038	1.3158

[a] In winter the outside surface resistance is taken as 0.029 m^2 °C/W.

Table 4
Constructions of the various structural components in the building envelope

Structural component	Layer sequence Left to right = inside to outside	U value (W/m^2 °C)
Exterior roof	i_H 6 1 8 9 4 3 0	1.670388
Exterior wall	i_V 6 7 2 5 0	1.808842
Exterior glass	i_V 10 0	5.888993
Exterior wooden door	i_V 11 0	2.087049
Exterior steel door	i_V 12 0	6.07040

The required regeneration temperature can be attained by a combination of multi-collectors in series and an auxiliary energy source. In the present work, the collector array is composed of 12 collectors in parallel and two collector rows in series.

The distribution of this array requires a modification of the house plan as shown in Fig. 24 by using a steel structure to support the collectors. This type of distribution highly reduces the effect of shading.

The storage capacity is taken as 0.3 m^3 per square meter of collector area. This value is consistent with typical values for solar air heating systems [2,13]. Attempting to increase the capacity above this value gives only insignificant increases in solar fraction as shown in Fig. 17.

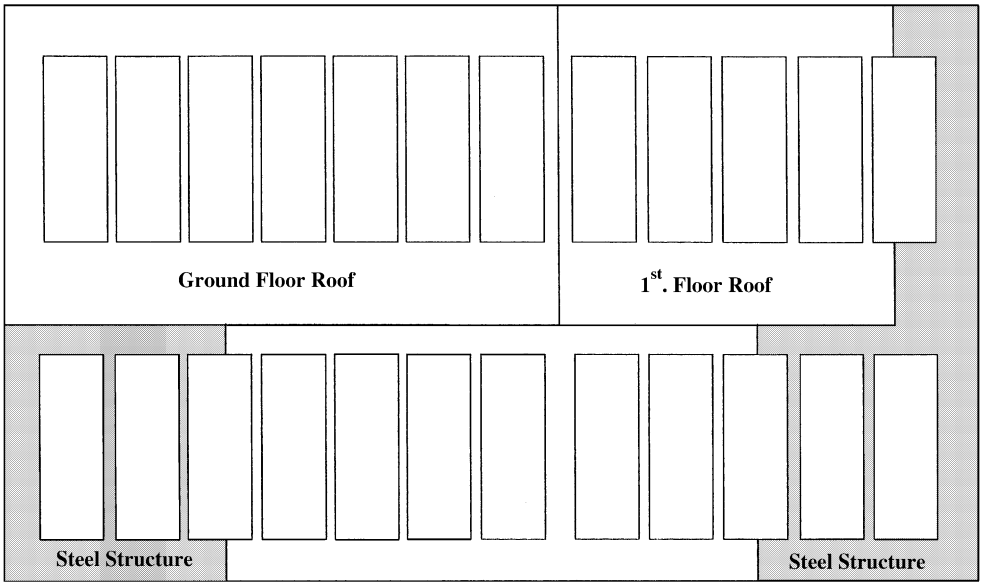

Fig. 24. Collectors distribution.

References

[1] Klein SA, et al. TRNSYS, A transient system simulation program, user's manual. Report no. 38, Engineering Experiment Station, University of Wisconsin, Madison, 1973.
[2] Beckman WA, Klein SA, Duffie JA. Solar heating design by the *f*-chart method. New York: Wiley; 1977.
[3] Kreider JF, Kreith F. Solar energy handbook. New York: McGraw Hill; 1981.
[4] Ajona JI, Gordon JM. An analytic model for the long-term performance of solar air heating systems. Solar Energy 1987;38(1):45.
[5] Duffie JA, Mitchell JW. *f*-chart predictions and measurements. Trans ASME J Solar Energy Engng 1983;105:3.
[6] Dunkle RV. A method of solar air conditioning. Mech Chem Engng Trans Inst Engrs Australia MC1 1965;1:73.
[7] Nelson JS, Beckman WA, Mitchell J, Close DJ. Simulation of the performance of open cycle desiccant system using solar energy. Solar Energy 1978;21:273.
[8] Van Leersum J. An analytical examination of open-cycle cooling systems. Trans ASME J Solar Energy Engng 1984;106:312.
[9] Kang TS, Maclain-Cross IL. High performance solid desiccant open cooling cycles. Trans ASME J Solar Energy Engng 1989;111:176.
[10] Crum DR, Mitchell JW, Beckman WA. Advanced desiccant cycles. Solar Energy Laboratory, University of Wisconsin, Madison, WI 53706.
[11] Joudi KA, Madhi SM. An experimental investigation into a solar assisted desiccant-evaporative air-conditioning systems. Solar Energy 1987;39(2):97.
[12] Oonk RL, Jones DE, Cole-Appel BE. Calculation of performance of *N* collector in series from test data on a single collector. Solar Energy 1979;23:535.
[13] Duffie JA, Beckman WA. Solar engineering of thermal process. New York: Wiley; 1980.
[14] Appelbaum J, Bany J. Shadow effects of adjacent solar collectors in large scale systems. Solar Energy 1979;23:497.
[15] Jones RE, Burkhart JF. Shading effect of collector rows tilted toward the equator. Solar Energy 1981;26:563.
[16] Bany J, Appelbaum J. The effect of shading on the design of a field of solar collectors. Solar Cells 1987;20:201.
[17] ASHRAE handbook of fundamentals. American Society For Heating Refrigeration, and Air-Conditioning Engineers Inc, New York, 1985.